Cooperative activated dynamics in dense mixtures of hard and sticky spheres

Douglas C. Viehman* and Kenneth S. Schweizer†
Department of Chemical and Biomolecular Engineering and Department of Materials Science, Frederick Seitz Materials Research Laboratory, University of Illinois, 1304 West Green Street, Urbana, Illinois 61801, USA
(Received 13 August 2008; published 21 November 2008)

The coupled activated dynamics in dense mixtures of repulsive and sticky hard spheres is studied using stochastic nonlinear Langevin equation theory. The effective free energy surface, barriers, saddle point trajectories, and mean first passage times depend in a rich manner on mixture composition, (high) total volume fraction, and attractive interaction strength. In general, there are three types of saddle point trajectories or relaxation pathways: a pure sticky or pure repulsive particle displacement keeping the other species localized, and a cooperative motion involving repulsive and attractive particle displacements. The barrier for activated hopping usually increases with the ratio of sticky to repulsive particle displacement. However, at intermediate values of the displacement ratio it can attain a broad plateau value, and can even exhibit a local maximum, and hence nonmonotonic behavior, at high sticky particle mixture compositions if the attraction strength is modest. The mean first passage, or hopping, times are computed using multidimensional Kramers theory. In most cases the hopping time trends reflect the behavior of the barrier height, especially as the sticky particle attraction strengths become large. However, there are dramatic exceptions associated with cooperative repulsive and attractive particle trajectories where the barriers are high but a greatly enhanced number of such trajectories exist near the saddle point.

DOI: 10.1103/PhysRevE.78.051404 PACS number(s): 82.70.Dd, 64.70.pv, 82.70.Gg

I. INTRODUCTION

The structure, equilibrium phase behavior, and nonequilibrium states (glass, gel) of colloidal and nanoparticle suspensions are of basic science and practical engineering interest [1–3]. For (effective) one-component fluids of attractive spheres major theoretical progress for predicting the emergence of kinetically driven gels and glasses has been achieved based on the ideal mode coupling theory (MCT) [4–7], a simplified version known as "naive MCT" (NMCT) [8–10], and a microscopic nonlinear stochastic Langevin equation (NLE) theory that goes beyond MCT to treat activated barrier hopping and non-Gaussian dynamic heterogeneity phenomena [9,11–14]. Very recently, we have generalized the NMCT and NLE approaches to mixtures of spherical particles [15]. A basic issue is colocalization of both species versus a partial transition where only one species localizes and the other diffuses as in a fluid [15–22].

Our present interest is "biphasic mixtures" [23] composed of equal diameter spheres where one species interacts solely via hard core repulsions, and the other experiences strong short range attractions. In their nanoparticle realization, the biphasic mixtures are composed of barium titanate particles which are coated with different polymers such that under the appropriate solvent conditions purely repulsive or (very short range) attractive interactions are achieved. The model colloidal biphasic mixtures are based on silica where the solvent dielectric properties, a hydrophobic organic coating, and surface charge are manipulated to realize (nearly) hard sphere and attractive interactions. Recent experimental studies of nanoparticle and colloid suspensions of such mixtures have discovered novel elasticity and nonlinear yielding behavior that allows major improvements in using concentrated particle suspensions in direct-write assembly applications [23]. Time-resolved confocal microscopy suggests highly asymmetric dynamics as the sticky particles are effectively solidlike on the experimental time scale and only the repulsive particles are mobile. Additional fundamental questions of interest include how vitrification and gelation interfere, what is the effect of repulsive particle excluded volume on gel elasticity and slow dynamics, and how does the formation of an ideal gel modify the repulsive particles tendency to localize and flow?

Our initial work [15] developed the basic theoretical approach, established the connection of NMCT to the full ideal MCT version [16–22], and presented a few preliminary numerical results. A mixture composition sensitive "glass-melting" type of kinetic arrest phenomenon is predicted at high total packing fractions and weak attractions. Complex behavior of the localization lengths and shear moduli occur as a consequence of the competition between excluded volume caging forces and attraction-induced physical bond formation. Beyond the NMCT ideal nonergodicity transition, a two-dimensional nonequilibrium free energy surface emerges that quantifies cooperative activated barrier hopping. This dynamical "landscape" has a rich structure with barrier locations and heights that are sensitive to the relative amplitude of the cooperative displacements of the sticky and repulsive particles.

In this paper, we present the first detailed numerical study of activated transport in highly concentrated biphasic mixtures. Section II briefly reviews the theory and summarizes multidimensional Kramers theory. The effective free energy surface is systematically studied in Sec. III as a function of the sticky particle attraction strength, total volume fraction, and mixture composition. Section IV computes mean first

*Present address: School of Chemistry, Georgia Institute of Technology, Atlanta, GA 30332.
†kschweiz@illinois.edu

passage times for various saddle point trajectories and provides a mechanistic picture for structural relaxation in glass and gel-like mixtures. The paper concludes in Sec. V. Tables of pertinent numerical results are collected in the Appendix.

II. THEORY AND MODEL

Naive mode coupling theory and the nonlinear Langevin equation approach are briefly reviewed for binary mixtures. Their physical motivation and further technical details have been previously discussed in depth [15].

A. Naive mode coupling theory

The key quantity of NMCT is the long-time limit of the force-force time correlation function exerted on a particle of species α by its surroundings, which in a Fourier space representation is given by [15]

$$\langle \mathbf{f}_\alpha(0)\cdot\mathbf{f}_\alpha(t)\rangle = \frac{1}{3\beta^2}\int \frac{d\mathbf{q}}{(2\pi)^3} q^2 e^{-q^2 r_{L,\alpha}^2/6} \times \sum_{j,k=1}^{2} C_{\alpha j}(q) S_{jk}(q,t) C_{k\alpha}(q), \quad \alpha = 1,2. \tag{1}$$

The long-time limit of the mean square displacement or localization length $r_{L,\alpha}$ is the ensemble-averaged dynamic order parameter, and a Gaussian Debye-Waller factor is employed. The effective intermolecular forces enter via the direct correlation function between species i and j, $C_{ij}(q)$, and $S_{ij}(q,t\to\infty)$ is the long-time limit of the partial dynamic structure factors which depend on the localization lengths [15]. The dynamic order parameters are related via two coupled self-consistency equations

$$\frac{1}{r_{L,\alpha}^2} = \frac{1}{9}\int \frac{d\mathbf{q}}{(2\pi)^3} q^2 e^{-q^2 r_{L,\alpha}^2/6} \sum_{j,k=1}^{2} C_{\alpha j}(q) S_{jk}(q,t\to\infty) C_{k\alpha}(q), \quad \alpha = 1,2. \tag{2}$$

The elastic shear modulus for a multicomponent system follows as [24]

$$G' = \frac{k_B T}{60\pi^2}\sum_{\gamma,\gamma'=1}^{2}\sum_{\delta,\delta'=1}^{2}\int_0^\infty dq q^4 \frac{dC_{\gamma\delta}(q)}{dq}\frac{dC_{\gamma'\delta'}(q)}{dq} \times S_{\gamma\gamma'}(q,t\to\infty) S_{\delta\delta'}(q,t\to\infty). \tag{3}$$

B. Nonlinear Langevin equation theory

For an (effective) one-component system, from heuristic physical arguments [9], and subsequently a statistical mechanical derivation based on local equilibrium and dynamic density functional concepts at the lightly coarse-grained dynamical variable level [11], NMCT has been generalized to account for single particle activated barrier hopping. For a binary mixture, the two coupled NLEs for the instantaneous scalar displacement of each species from their initial position $r_\alpha(t)$ are [15]

$$-\zeta_{s,\alpha}\frac{d}{dt}r_\alpha - \frac{\partial}{\partial r_\alpha}F_{\rm eff}(r_1,r_2) + \delta f_\alpha = 0, \quad \alpha = 1,2,$$

$$\langle \delta f_\alpha(0)\delta f_\gamma(t)\rangle = 2k_B T\zeta_{s,\alpha}\delta_{\alpha\gamma}\delta(t), \tag{4}$$

where $\zeta_{s,\alpha}=k_BT/D_{s,\alpha}$ is the short-time friction constant for species α, $D_{s,\alpha}$ is the corresponding short-time diffusion constant, $\delta f_\alpha(t)$ is the white noise random force, and $F_{\rm eff}(r_1,r_2)$ is an effective or nonequilibrium "free energy" surface given by [15]

$$F_{\rm eff}(r_1,r_2) - F_{\rm eff}(r_{L,1},r_{L,2}) = \int_{r_{L,1}}^{r_1}\frac{\partial F_{\rm eff}(r_1,r_2)}{\partial r_1}dr_1 + \int_{r_{L,2}}^{r_2}\frac{\partial F_{\rm eff}(r_1,r_2)}{\partial r_2}dr_2, \tag{5}$$

$$\frac{\partial}{\partial r_\alpha}F_{\rm eff}(r_1,r_2) = \beta\langle \mathbf{f}_\alpha(0)\cdot\mathbf{f}_\alpha(t\to\infty)\rangle_{r_1,r_2} r_\alpha - 3k_BT/r_\alpha, \quad \alpha = 1,2, \tag{6}$$

where $\langle\cdots\rangle_{r_1,r_2}$ refers to the $t\to\infty$ limit of Eq. (1) with the ensemble-averaged quantity $r_{L,\alpha}$ replaced by the dynamical variable r_α. In general, stochastic trajectories of the different species are coupled corresponding to correlated motion. However, for many cases of practical interest a high dynamical asymmetry is relevant and the theory simplifies [15]. The NLE theory crosses over to an effective Fickian diffusion description at long enough times and displacements [12], the detailed formulation of which is not important for the present work.

If the noise in Eq. (4) is dropped and the dynamical variables are replaced by their ensemble-averaged localization lengths, then ideal NMCT is recovered [9,11]. In the context of the NLE approach, the ideal kinetic arrest transition represents a crossover to activated barrier hopping controlled dynamics where ergodicity is always attained in the long-time limit.

C. Biphasic mixture model and structural correlations

A biphasic mixture consists of repulsive and attractive spheres of identical diameter (D) that interact via hard core repulsions. We refer to repulsive particles with the letter "g" for "glassy" and the attractive particles with "s" for "sticky." The g-g and g-s interactions are purely hard core. The sticky particles also interact via an exponentially decaying attraction

$$v_{ss}(r) = -\varepsilon_{ss}\exp\left(\frac{D-r}{a}\right), \quad r \geqslant D, \tag{7}$$

where ε_{ss} is the contact strength. In this paper the spatial range parameter is fixed at $a=0.02D$, which corresponds to $\sim$1 nm for the $D=60$ nm nanocolloids recently studied experimentally [23]. Our focus is on dense mixtures, and the total volume or packing fraction is chosen to be $\phi_T=0.45$ or 0.5. The sticky particle composition ϕ_s varies from zero to unity. The structural pair correlations are computed from the

mixture Ornstein-Zernike equation with the Percus-Yevick closure [25]

$$h_{ij}(r) = C_{ij}(r) + \sum_{k=1}^{2} \int d\mathbf{r} C_{ik}(\mathbf{r}-\mathbf{r}')\rho_k h_{kj}(\mathbf{r}'), \tag{8}$$

$$C_{ij}(r) = (e^{\beta v_{ij}(r)} - 1)g_{ij}(r), \quad r > D,$$

$$g_{ij}(r) = 0, \quad r < D, \tag{9}$$

where $g_{ij}(r)=1+h_{ij}(r)$ is the radial distribution function between species i and j. The integral equations are solved numerically using the Picard algorithm [25].

D. Limiting case

For biphasic mixtures the attractive particle motion is often far slower than its repulsive particle counterpart. This motivates consideration of a simpler "two-step" description [15] involving a pair of one-dimensional effective free energy functions. At long enough times, the fast species escape their dynamical constraints and become liquidlike from the perspective of the slow particles. The dynamics of the latter is then treated as a psuedo-one-component system where the fast species enters implicitly via an effective direct correlation function [10,26] determined by the full two-component structural correlations. Equation (2) then reduces to a single NMCT equation given by [10,15]

$$r_{L,s}^{-2} = \frac{1}{9} \int \frac{d\mathbf{q}}{(2\pi)^3} q^2 C_{ss,\mathrm{eff}}^2(q) S_{ss}(q) e^{-(q^2 r_{L,s}^2/6)[1+\rho_s/S_{ss}(q)]}, \tag{10}$$

where [27]

$$S_{ss}(q)/\rho_s = \frac{1-\rho_g C_{gg}(q)}{1-\rho_g C_{gg}(q) - \rho_s C_{ss}(q) + \rho_g \rho_s [C_{gg}(q)C_{ss}(q) - C_{sg}^2(q)]} \tag{11}$$

and $C_{ss,\mathrm{eff}}(q)$ is the "effective" direct correlation function for the slower sticky species

$$C_{ss,\mathrm{eff}}(q) = \frac{1}{\rho_s} - \frac{1}{S_{ss}(q)}. \tag{12}$$

The corresponding scalar NLE and effective free energy have the form of a one-component system extensively considered previously [9,11,14] which is expressed in terms $C_{ss,\mathrm{eff}}(q)$ and $S_{ss}(q)$. The mean first passage, or barrier "hopping," time in the high friction, diffusive limit of interest is given by [9,28]

$$\frac{\tau}{\tau_0} = \frac{2\pi G}{\sqrt{K_0 K_B}} e^{F_B}, \tag{13}$$

where F_B is the barrier height in units of the thermal energy, the absolute magnitudes of the well and barrier curvatures are K_0 and K_B (units of k_BT/D^2), respectively, and $G \equiv \zeta_s/\zeta_0$ is the ratio of the short-time friction constant to its dilute limit analog which is the Stokes-Einstein result for a colloidal suspension [1]. For hard spheres, G is well described by the contact value of the radial distribution function $g(r=D)$, which quantifies binary collisions [25,29]. The mean first passage time has been nondimensionalized by the elementary Brownian diffusion time $\tau_0=\beta\sigma^2\zeta_0$.

E. Multidimensional Kramers theory

Langer [30] generalized Kramers theory to many degrees of freedom based on the idea that the system follows a saddle point trajectory corresponding to a path of least resistance on the effective free energy surface. For biphasic mixtures, multiple trajectories may be relevant in the sense that the characteristic first passage times are comparable. These represent mechanistically different motions for escaping dynamical constraints, influenced by both the barrier and an entropic factor associated with the "width" of the saddle point region. Curvatures of the free energy surface at both the localized state minimum and at the saddle point enter the "reaction rate" calculation.

The mean first passage time is given by [28,30,31]

$$\frac{\tau}{\tau_0} = \frac{2\pi}{\lambda^+} \left(\frac{|\det \mathbf{K}_B|}{\det \mathbf{K}_0} \right)^{1/2} \exp(F_B), \tag{14}$$

where $\mathbf{K}_B$ is the matrix of second derivatives at the saddle point, $\mathbf{K}_0$ is the matrix of second derivatives at the NMCT localization length, and λ^+ is the sole positive eigenvalue to the characteristic equation $\det(\mathbf{I}+\mathbf{D}\cdot\mathbf{K}_B)$ where $\mathbf{D}$ is the matrix of short-time diffusion coefficients and $\mathbf{I}$ is the identity matrix. $\mathbf{D}$ is related to the short-time friction constants $D_{s,i}=1/\zeta_{s,i}=1/G_i\zeta_0$. We determine $D_{s,i}$ based on an Enskog hard sphere mixture model [14,25,29], where the collision rates are modified by the intermolecular attractions and structure via the contact values of radial distribution functions. Specifically, a diagonal short time diffusion constant matrix is employed with $G_s=\phi_s g_{ss}(r=D)+\phi_g g_{gs}(r=D)$ for attractive particle displacements and $G_g=\phi_g g_{gg}(r=D)+\phi_s g_{gs}(r=D)$ for repulsive particle displacements. In the numerical applications presented below, the contact values and $g_{gs}(D)$ are roughly the same while $g_{ss}(D)$ may be up to an order of magnitude higher due to attractive particle clustering.

III. EFFECTIVE FREE ENERGY SURFACES

The effective or dynamical free energy surface depends on the strength of sticky particle attraction ε_{ss} and mixture composition at a high total packing fraction of 0.45 or 0.5. Except for the NMCT ideal kinetic arrest diagram of Fig. 1, ε_{ss} varies over the range of $2.75k_BT$–$4k_BT$. Throughout the rest of the paper, and in all figures and tables, energy is expressed in units of k_BT and length in units of the particle diameter D.

A. Ideal kinetic arrest phase diagram

Figure 1 shows the ideal nonergodicity boundaries for $\phi_s=0.25$, 0.50, 0.75, and 1.0. The $\varepsilon_{ss}\to 0$ or $\phi_s\to 0$ limit corresponds to a hard sphere fluid where [9] the ideal NMCT

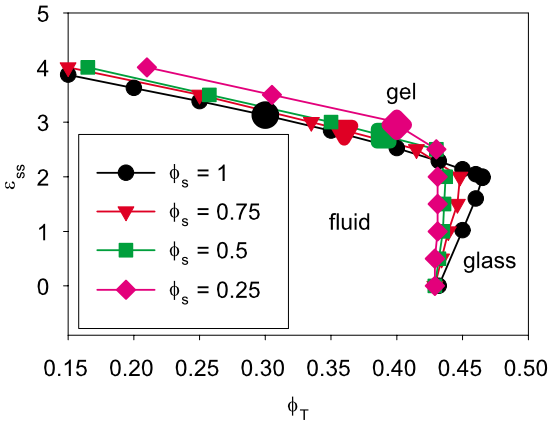

FIG. 1. (Color online) Naive MCT ideal kinetic arrest diagram in the format of attraction strength (units of k_BT) versus total packing fraction for biphasic mixtures with attractive particle compositions of 25%, 50%, 75%, and 100%, represented by diamonds, squares, upside-down triangles, and circles, respectively. Solid curves are guides to the eye. The large data points indicate a crossover from double localization (to the right) to only attractive particle localization (to the left).

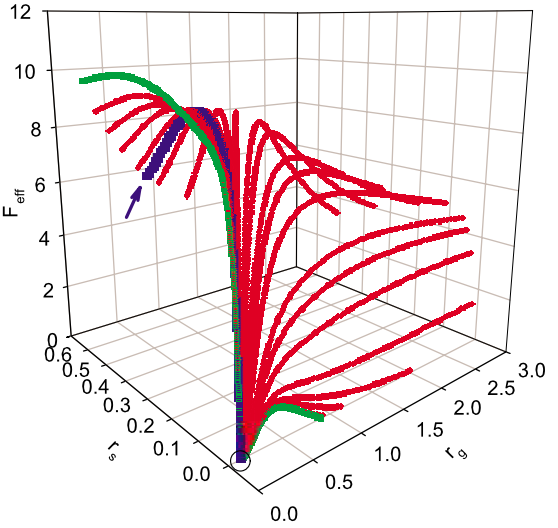

FIG. 2. (Color online) Effective free energy surface as a function of repulsive and attractive particle displacements (units of particle diameter D) for total volume fraction of 0.45, composition of 50%, and attraction strength of $3k_BT$. The circle denotes the (transient) localized state, and the arrow indicates the $\delta r_s/\delta r_g=1$ cooperative trajectory.

glass transition occurs at $\phi_T=0.432$ with a localization length of $\sim 0.18D$. As sticky particles are added at low attraction strengths, the nonergodicity boundary shifts to larger total packing fractions in a manner that becomes more dramatic with increasing ϕ_s. This reentrant behavior is reminiscent of the "glass melting" phenomenon predicted by one-component MCT, and experimentally observed, for attractive colloids [3,4,7].

For an attraction strength of $\sim 2.5k_BT$ and larger, the nonergodicity lines for the various compositions cross and undergo a reversal of direction, resulting in a "noselike" feature. A monotonic reduction of the total packing fraction at the NMCT transition with increasing strength of attraction occurs, and the kinetic arrest boundary varies linearly with ε_{ss} and is rather weakly dependent on composition. The large symbols on each curve indicate a critical value of total packing fraction below which the repulsive species undergoes a discontinuous transition from a localized state to a delocalized fluid [15].

It is interesting to ask whether at high total volume fractions, but below the nonmonotonic glass melting region, there are any similarities of the biphasic mixture results in Fig. 1 with a recent ideal MCT study of hard-sphere fluids confined in a quenched disordered porous matrix of identical hard spheres [32]. The model porous medium consists of pinned hard spheres at a volume fraction ϕ_m, and a mobile fluid of volume fraction ϕ_f; the total particle volume fraction is $\phi_T=\phi_m+\phi_f$. For this system ideal MCT predicts a nonmonotonic or reentrant form for the kinetic arrest diagram in a ϕ_m versus ϕ_f representation, but for $\phi_m \leqslant 0.175$ there is a single value of ϕ_f for each ϕ_m. Over the rather wide range of $0.05 \leqslant \phi_m \leqslant 0.175$, ϕ_f at the ideal nonergodicity transition is given by $0.43 \geqslant \phi_f \geqslant 0.22$, respectively. However, in the format of Fig. 1, the total volume fraction in Ref. [32] (mobile plus quenched hard spheres) along the ideal glass transition boundary is nearly constant, $\phi_T \cong 0.44 \pm 0.04$, despite the fact that the fraction (composition) of frozen matrix particles, $\Phi \equiv \phi_m/\phi_T$, varies over a wide range from $\sim 10\%$ to 45%. These results appear to be qualitatively similar to the biphasic mixture kinetic arrest transition boundaries in Fig. 1 in the sense that for $\phi_T \approx 0.41-0.43$ the ideal nonergodicity boundary is nearly composition (ϕ_s) independent. Hence, the sticky particles in biphasic mixtures can possibly be viewed as providing an effectively porous medium, which can induce repulsive particle localization.

Although our present focus is high total particle volume fraction mixtures, one can ask what is the meaning of the ideal MCT gel boundaries in Fig. 1 at relatively low ϕ_T. This is a complicated question since at low total volume fractions the kinetic gelation process may be coupled with cluster aggregation and/or macroscopic phase separation [2,3]. Prior applications of naive MCT for ideal gel boundaries and elastic shear moduli for depletion systems agree well with experiments [10]. However, the ideal gel line represents a dynamical crossover to an ultraslow activated motion regime [14], and in the lower volume fraction regime the associated physics in the NLE theory has not been extensively explored.

B. Effective free-energy surfaces

The dynamical free-energy surface is a function of repulsive and sticky particle displacements, r_g and r_s, respectively. Figure 2 shows the surface for $\phi_T=0.45$, $\phi_s=0.5$, and $\varepsilon_{ss}=3$. Its shape is strongly dependent on the relative particle displacements, i.e., the "direction" of a trajectory on the two-dimensional landscape. Now consider the initial state is at the minimum of the effective free energy corresponding to the NMCT localized state (circle in Fig. 2). Solution of the NLEs will result in cooperative motion of the two species that can be characterized by the ratio of displacements from the localized state, $\delta r_s/\delta r_g$. This ratio varies from zero for a

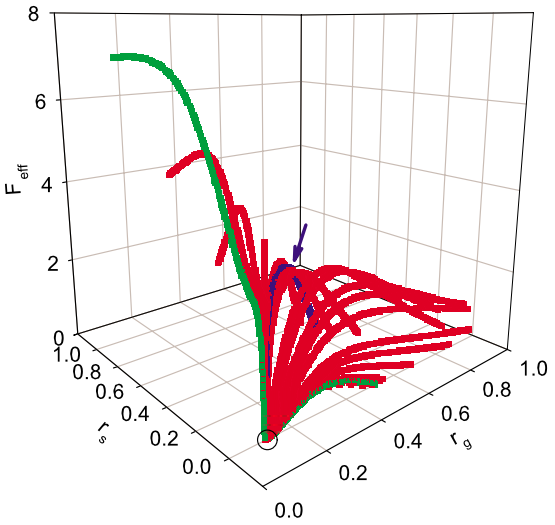

FIG. 3. (Color online) Effective free energy surface as a function of repulsive and attractive particle displacement for a total volume fraction of 0.45, attractive particle composition of 20%, and attraction strength of $3k_BT$. The circle denotes the (transient) localized state, and the arrow denotes the $\delta r_s/\delta r_g=1$ cooperative trajectory.

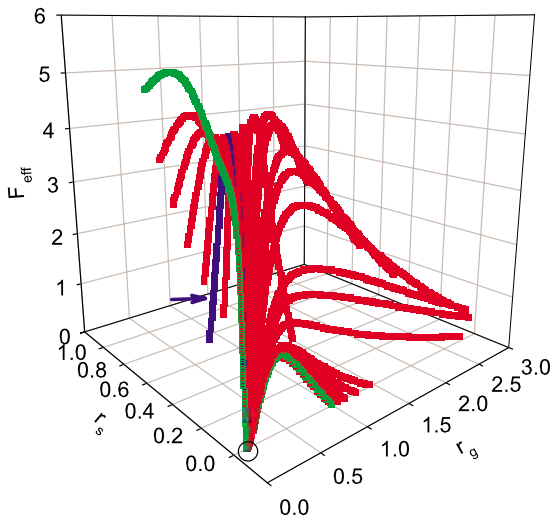

FIG. 4. (Color online) Effective free energy surface as a function of repulsive and attractive particle displacements for total volume fraction of 0.45, composition of 50%, and attraction strength of $2.75k_BT$. The circle denotes the (transient) localized state, and the arrow indicates the $\delta r_s/\delta r_g=1$ cooperative trajectory.

pure repulsive particle displacement to infinity for a pure attractive particle displacement. The barrier curvature and height are strongly dependent on displacement ratio.

For a pure attractive particle displacement, $F_B\sim 10$ for the system in Fig. 2 corresponding to slow activated transport. When r_g changes by the same amount as r_s ($\delta r_s/\delta r_g=1$ as indicated by the arrow in Fig. 2), the barrier is only slightly lowered to 9.2. The reason is that significant displacement of attractive particles requires "physical bond" breakage. The barrier does decrease sharply as sticky particle displacements become very small compared to their repulsive counterparts as indicated by the wall of curves near and along the r_g axis. For example, $F_B\sim 8$ when $\delta r_s/\delta r_g\sim 0.07$, and ~ 5 for $\delta r_s/\delta r_g\sim 0.016$. For these latter cases, the dominant displacement corresponds to repulsive particle motion; however, small displacements of the attractive species still have a major effect. Since $F_B\sim 1k_BT$ for a pure repulsive particle displacement, it would appear to be the primary path explored during the initial stage of activated dynamics. However, we demonstrate in Sec. IV that this is not the only relevant trajectory.

Figure 3 illustrates how the effective free-energy surface changes if the sticky particle composition is lowered to $\phi_s=0.2$. With increasing repulsive particle displacement, $F_{\text{eff}}(r)$ now decays quickly from its peak value of 7 (pure sticky particle displacement) as the steric blocking of attractive particles is greatly reduced. A relatively flat plateau exists at an intermediate displacement ratio that indicates significant cooperative motion is likely for entropic reasons. The lowest barrier of 0.55 occurs for a pure repulsive particle displacement.

The rather large consequences of modestly reducing the attraction strength by $0.25k_BT$ is shown in Fig. 4 for $\phi_s=0.5$. The maximum barrier is roughly halved (~ 5) compared to its analog in Fig. 2 for a pure attractive particle displacement. The barrier is lowest, $F_B\sim 1.2$, for a pure repulsive particle displacement. Interestingly, this is slightly higher than its analog for the $\varepsilon_{ss}=3$, $\phi_s=0.5$ mixture in Fig. 2. A local minimum of the barrier as a function of relative displacement of height 4.3 emerges for roughly equal displacements of repulsive and attractive particles. Unlike in Fig. 2, the decrease in barrier height is much more gradual as the displacement ratio $\delta r_s/\delta r_g$ decreases.

C. Barrier heights and locations

The nonequilibrium free-energy surfaces discussed above suggest that a pure attractive (repulsive) particle displacement encounters the highest (lowest) barrier. A pure repulsive particle displacement models an effective porous medium since the attractive particles remain localized over experimentally relevant time scales. We previously showed [15] the barriers for pure repulsive and attractive displacements follow an apparent power law function of total volume fraction as measured from its ideal NMCT value, $\phi_T-\phi_c$: $F_B\sim(\phi_T-\phi_c)^y$ where $y\sim 1.7$ (1.45) for pure attractive (repulsive) particle displacement.

Figure 5 presents calculations of the barrier height as a function of the relative displacement ratio for three mixture compositions at fixed $\varepsilon_{ss}=3$ and total packing fraction. The barrier height generally grows with increasing attractive particle displacement. However, for $\phi_s=0.8$, the barrier is a nonmonotonic function with a maximum of 10.8 occurring at $\delta r_s/\delta r_g=0.12$. As expected, F_B monotonically grows with sticky particle composition in the pure repulsive particle displacement limit. In the pure attractive particle displacement limit, however, the barrier height is a nonmonotonic function of composition. This presumably reflects competing factors at high attractive particle compositions: fewer immobile repulsive particles and enhanced clustering of sticky spheres, which can open up more free volume. For all compositions,

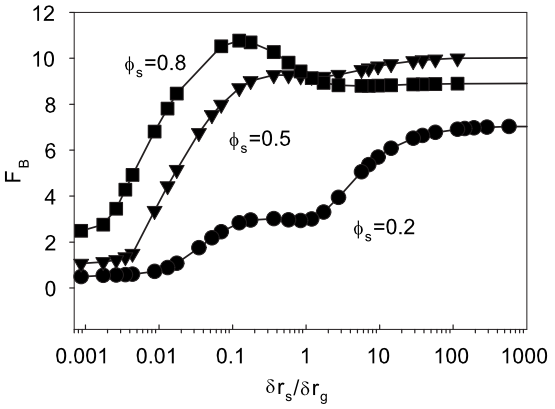

FIG. 5. Barrier heights (units of k_BT) as a function of relative particle displacement variable for a mixture with a total volume fraction of 0.45, attractive particle compositions of 20%, 50%, and 80% (circles, triangles, and squares, respectively), and an attraction strength of $3k_BT$.

F_B grows roughly logarithmically with $\delta r_s/\delta r_g$ for primarily repulsive particle displacement motions corresponding to $\delta r_s/\delta r_g=0.01-0.1$. For primarily attractive particle displacements of $\delta r_s/\delta r_g \sim 1-10$, there is a strong ϕ_s dependence of the barrier height in response to changing displacement ratio.

An example of the effect of sticky particle attraction strength on the barrier for single species displacements is shown in Fig. 6 for $\phi_s=0.5$ and $\phi_T=0.45$. Here, the attractive particles form an ideal glass or gel for any magnitude of attraction. Note there is an order of magnitude increase of the barrier for a sticky particle displacement from $F_B \sim 2$ to 27 as ε_{ss} increases only from 2.5 to 3.5. In contrast, for a pure repulsive particle displacement the barrier decreases from 1.4 to 0.7 as ε_{ss} increases. The reason is that the attractive particles are more localized at higher ε_{ss}, which opens up additional space for repulsive particle motion.

The results in Figs. 2–6 hint at additional interesting and complex variations of the barrier height and location r_B as the mixture composition is changed at fixed attraction strength and volume fraction. Figure 7 shows nonmonotonic behavior of F_B for a pure attractive particle displacement when $\phi_T=0.45$ and $\varepsilon_{ss}=3$. The minimum value of $F_B \sim 5.6$ occurs close to the composition where attractive particles begin to form an ideal gel ($\phi_s=0.12$). Beyond this composition F_B increases with growing ϕ_s since the sticky particles form a stronger gel-like material. However, it is not as intuitive as to why the barrier for attractive particle motion increases when ϕ_s decreases toward zero. The reason is that repulsive particles are localized for the trajectory considered, and they present more immobile steric obstacles for sticky particle motion as their number increases. For mixtures that can form gels, the interplay between increased attractive particle aggregation and repulsive particle blocking effects impeding sticky particle motion results in a local barrier maximum of ~ 10 at the intermediate composition $\phi_s=0.5$. At even higher attractive particle compositions, the reduction of localized repulsive particles lowers the barrier because the sticky particles cluster more and further increasing their number does not significantly modify the degree of localization.

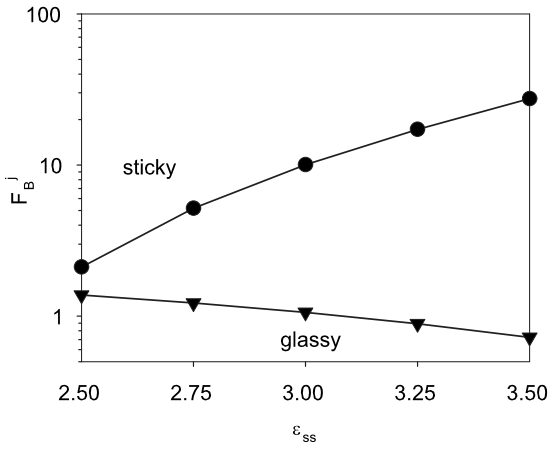

FIG. 6. Barrier heights for pure repulsive and pure attractive displacements as a function of attraction strength for a mixture with a total volume fraction of 0.45 and attractive particle composition of 50%.

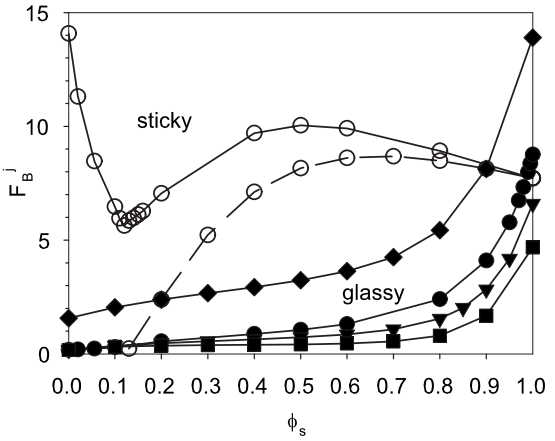

FIG. 7. Barrier heights for pure repulsive and pure attractive displacements as a function of sticky particle composition. The open circles are for pure attractive particle displacements, attraction strength of $3k_BT$, and a total volume fraction of 0.45. The solid curve with open circles are results for when the repulsive particles are trapped at their localization lengths. For the dashed curve, the repulsive particles are an equilibrated fluid. The solid symbols (circles, upside-down triangles, squares) are for pure repulsive particle displacements with parameters as above except attraction magnitudes (from top to bottom) are 3, 3.5, and 4. The solid diamonds are a mixture with a total volume fraction of 0.5 and attraction strength of 3.

In general, we do not expect pure attractive particle displacements will thermally occur on a similar time scale as repulsive particle activated motion. A more likely scenario is the repulsive particles escape their cages and "fluidize" long before the attractive particles undergo activated motions. Results under this limiting condition (see Sec. II D) are also shown in Fig. 7 as the dashed curve. Now the counterintuitive results discussed above for barrier heights associated with sticky particle displacement at low values of ϕ_s no longer occur. At higher values of ϕ_s where there are few immobile repulsive particles, the barrier is only slightly

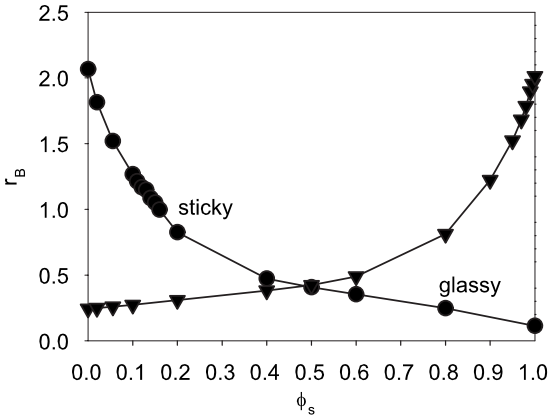

FIG. 8. Barrier locations for pure repulsive and pure attractive displacements as a function of mixture composition with a total volume fraction of 0.45 and attraction strength of $3k_BT$.

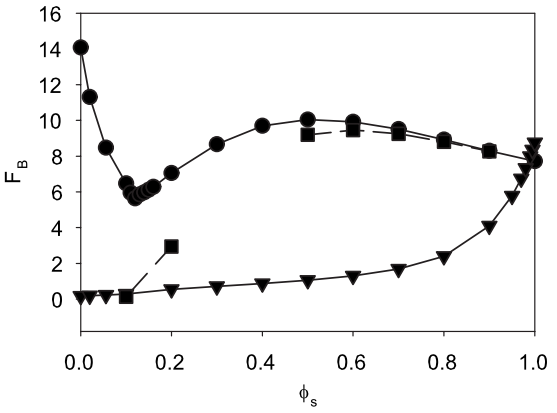

FIG. 9. Barrier heights for pure repulsive (inverted triangles), pure attractive (circles), and (if present) cooperative (squares) displacement saddle point trajectories as a function of mixture composition with a total volume fraction of 0.45 and attraction strength of $3k_BT$.

smaller than its pure attractive particle displacement analog in the mixture.

The solid curves in Fig. 7 also show the barrier height for pure repulsive particle displacements as a function of mixture composition. The lower three curves (top to bottom) are for $\varepsilon_{ss}=3$, 3.5, and 4, respectively, and are qualitatively similar with F_B monotonically increasing with sticky particle composition. As suggested by Fig. 6, F_B decreases with increasing ε_{ss} due to enhanced sticky particle localization and aggregation, which opens up more free volume for repulsive particles. The top solid curve is for a $\phi_T=0.5$ system with $\varepsilon_{ss}=3$. A much steeper increase in F_B occurs due to tighter caging of the repulsive particles.

The location of the barriers for pure species displacements are of interest since they define the "transition state." Figure 8 shows results as a function composition for $\phi_T=0.45$ and $\varepsilon_{ss}=3$. The most striking feature is the near mirror image nature of the sticky and repulsive particle curves. The barrier location is also a dramatic function of ϕ_s and can be greater than the particle diameter for both species due to severe steric blocking when the mobile particles become dilute. We find (not shown) the repulsive particle barrier location correlates with the location of the first minimum of the radial distribution function, $g_{gg}(r)$; small adjustments in $g_{gg}(r)$ make large differences in the barrier locations. For example, as the first minimum in $g_{gg}(r)$ shifts from 1.51 to 1.70 particle diameters the barrier location shifts from 0.4 to over $2D$.

In addition to the pure attractive and repulsive particle displacement trajectories, we find that a saddle-point trajectory in the effective free energy exists at intermediate values of $\delta r_s/\delta r_g$ corresponding to cooperative motion of the two species for many mixture compositions at modest attraction strengths. Figure 9 shows barrier heights for such a cooperative saddle point, and pure repulsive and attractive species displacement, trajectories when $\phi_T=0.45$ and $\varepsilon_{ss}=3$. In addition, Table I in the Appendix presents a summary of barrier heights and locations, localization lengths, and shear moduli. For both low and high values of ϕ_s, a cooperative motion trajectory exists. For all the mixtures studied, a maximum of one cooperative motion trajectory has been found. For low attractive species compositions, the repulsive particle is the primary displacement; for example, at $\phi_s=0.2$, $\delta r_s/\delta r_g=0.87$, and $F_B=2.94$. For intermediate values of ϕ_s, no highly cooperative saddle points are found since their effective free-energy surfaces are monotonically decreasing with increasing $\delta r_s/\delta r_g$. The cooperative saddle-point trajectories reemerge at high ϕ_s but are nearly identical to the pure attractive displacement analog with slightly smaller barriers.

The bottom of Table I shows results at other attraction strengths. For $\varepsilon_{ss}=2.75$, a saddle trajectory where both species significantly displace does exist at $\phi_s=0.5$ and 0.8, and barriers are ~5 or less. For these mixtures, motion of the repulsive and attractive particles should be highly cooperative. For $\varepsilon_{ss}=3.5$ and $\phi_s=0.8$, a cooperative displacement trajectory also appears but has a barrier only $0.1k_BT$ lower than its pure attractive displacement analog of 21.6. Since the barrier for a pure repulsive displacement is only 1.5, the effective free-energy surface is highly asymmetrical, and one expects repulsive particle displacements dominate the initial relaxation process.

D. Localization length and shear modulus

The results in Table I in the Appendix demonstrate that for the $\varepsilon_{ss}=3$ systems there is a significant decrease in attractive particle localization length once the ideal MCT gelation threshold is first reached. All mixtures beyond $\phi_s=0.1$ have a much smaller localization length that varies nonmonotonically, and there is a corresponding jump in the elastic shear modulus, G'. As the attractive particle composition increases, there are fewer repulsive particles to sterically push sticky spheres close together. The shear modulus increases rapidly once a gel forms, is dominated by the contribution of attractive particles, and monotonically increases with ϕ_s, but tends to saturate at high attractive particle compositions. For example, $G' \sim 17k_BT/D^3$ for a pure repulsive mixture, grows to $\sim 5000k_BT/D^3$ at $\phi_s=0.2$, and peaks at $74\,600k_BT/D^3$ for a pure attractive particle gel.

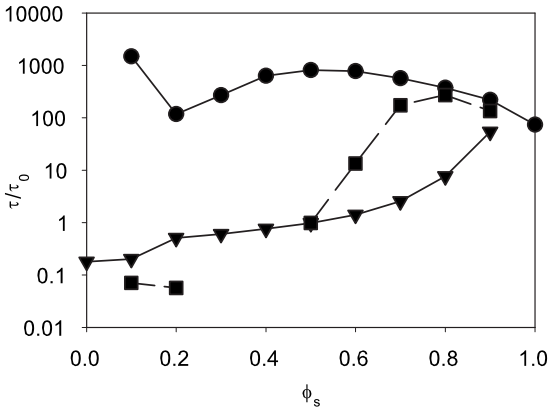

FIG. 10. Mean first passage times for pure repulsive (inverted triangles), pure attractive (circles), and cooperative motion (squares; if applicable) saddle point trajectories as a function of mixture composition with a total volume fraction of 0.45 and attraction strength of $3k_BT$.

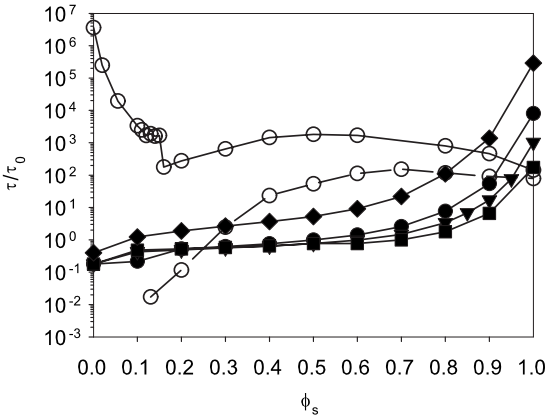

FIG. 11. Mean first passage times for pure repulsive and attractive displacements as a function of mixture composition; the same labeling scheme as in Fig. 7 applies.

IV. BARRIER HOPPING TIME SCALES AND COOPERATIVE DYNAMICS

We now apply Eq. (14) to compute the mean barrier hopping time for all saddle paths on the two-dimensional surface. For one-component systems this time scale has been demonstrated to be closely related to the alpha relaxation time in the glassy regime [9,12].

Figure 10 shows the mean first passage time associated with pure repulsive, pure attractive, and cooperative (when it exists) saddle-point trajectories for the $\phi_T=0.45$ and $\varepsilon_{ss}=3$ mixture. Table II in the Appendix collects the factors that enter the rate calculation and presents results for two additional attraction magnitudes of $\varepsilon_{ss}=2.75$ and 3.5. When $\varepsilon_{ss}=3$, the barrier hopping times for pure species displacements qualitatively follow the F_B trends in Fig. 9, i.e., τ/τ_0 grows roughly exponentially with barrier height. However, for the collective motion the hopping times are clearly not solely controlled by the barrier height. At low ϕ_s, the cooperative motion hopping time is shorter than that of a pure repulsive particle displacement, even though the corresponding barrier is larger. Furthermore, these hopping times deviate significantly from the pure attractive displacement analog even when their corresponding barrier heights are similar. This is particularly noteworthy at intermediate values of ϕ_s as now the cooperative motion trajectory has a mean first passage time within an order of magnitude of a pure repulsive displacement trajectory despite its much higher barrier. Clearly, this cooperative motion is an alternate path to mixture relaxation.

The relevance of the cooperative relaxation channel can be physically and mathematically understood by examining the "prefactor" column in Table II of the Appendix. At intermediate values of ϕ_s, F_B for the cooperative trajectory is roughly $8k_BT$ larger than its pure glassy displacement analog. If all preexponential terms in Eq. (14) were constant, this would increase the hopping time by a factor of 3000 and a pure glassy displacement would be the dominant relaxation channel. However, when the preexponential factor is considered for $\phi_s=0.5$, we find $\tau/\tau_0 \sim 1$ for the cooperative motion trajectory ($\delta r_s/\delta r_g=1.38$), which is essentially identical to its pure repulsive particle trajectory analog. Hence, the cooperative motion is a competitive relaxation channel due to the existence of many more paths in the vicinity of the barrier. The detailed mathematical reason is that at the saddle point the local curvatures for both pure attractive and repulsive displacement are relatively small, which significantly reduces $|\det \mathbf{K}_B|$ in Eq. (14). For the pure repulsive displacement trajectory, the curvature for an attractive particle displacement at the saddle point is very large and similar to the curvature at the localization length. Hence, saddle points that have roughly equal repulsive and attractive particle displacements are characterized by many more pathways for crossing the barrier. This aspect is clearly shown by the curve indicated by the arrow in Fig. 2, in contrast to the narrow path the pure repulsive particle displacement trajectory must follow. Table II also shows the attractive particle contact values are typically an order of magnitude higher than their repulsive analogs for most mixture compositions. This results in a relative reduction of the hopping time in Eq. (14) due to short-time frictional effects.

The results in Table II also demonstrate that if the attraction strength is lowered to 2.75, barriers for all saddle-point trajectories of the $\phi_s=0.8$ mixture are roughly equal. Moreover, the prefactor for a pure repulsive displacement is about ten times larger than any other displacement ratio path, which results in this trajectory having the largest hopping time. Conversely, if ε_{ss} is raised to 3.5, the barriers drastically increase and prefactor effects are negligible; the pure repulsive displacement trajectory dominates the other relaxation channels. Additional calculations (not shown) demonstrate that further increase of the sticky particle attraction strength completely quenches the competitiveness of alternative pathways.

Finally, we consider the hopping time trends for pure species displacement trajectories in Fig. 11 as a function of mixture composition for the same systems in Fig. 7. For $\varepsilon_{ss}=3$ and $\phi_T=0.45$, the repulsive particle displacement hopping time is not much larger than the Brownian time τ_0 for most mixture compositions. However, for high ϕ_s the mean hopping time increases very rapidly due to the presence of a

dense matrix of tightly localized sticky particles. A similar trend appears for the $\varepsilon_{ss}=4$ mixture, but the time scale is lower relative to the $\varepsilon_{ss}=3$ system since the attractive particles form tighter clusters, resulting in more free volume for repulsive particle motion. The composition dependence of the hopping time is supraexponential: $\tau/\tau_0 \propto \exp[a\phi_s^b]$, where $[a,b]=[1.06F_B(\phi_s=1),5.8]$ and $[1.24F_B(\phi_s=1),7.0]$ for the $\varepsilon_{ss}=3$ and 4 systems, respectively. Note also for the $\varepsilon_{ss}=3$ mixture at $\phi_T=0.45$, there is a small decrease in the hopping time at $\phi_s=0.1$ compared to the $\varepsilon_{ss}=3.5$ and 4 mixtures. This is because the attractive particles have not yet undergone an ideal gelation transition and hence they block the repulsive particles far less efficiently.

Comparing Fig. 11 to Fig. 7, major similarities exist between the barrier heights and mean first passage times for single species trajectories. To a first approximation all the trends are identical. Hence, prefactors enter in a minor manner, and the barrier height qualitatively controls the mean first passage times for pure repulsive displacements. Note that for the pure attractive particle displacements in the $\varepsilon_{ss}=3$ system of Fig. 11 (open circles, solid curve) there is drastically nonmonotonic behavior of the hopping time, which qualitatively follows similar trends as the barrier height trends in Fig. 7. The largest barrier hopping times exist when $\phi_s \to 0$ since the localized repulsive particles block attractive particle motion. Near the ideal gel transition, a local minimum of the mean passage time exists. Beyond this point, an increase in composition increases the hopping time because sticky particles become localized. Mean first passage times peak at $\phi_s \sim 0.5$ and mildly decrease with increasing ϕ_s as now clustering of attractive spheres saturates and there are fewer blocking repulsive particles.

As discussed above, repulsive particle localization on the time scale of attractive particle hopping motion is unlikely to occur in real mixtures. This motivates the presentation of "effective one-component" results in Fig. 11. The nonmonoticity of the barrier hopping times for attractive particle displacements at low ϕ_s then disappears. For higher values of ϕ_s, the hopping time follows the analogous result well when the repulsive particles remain localized. Therefore, when the repulsive spheres become dilute they contribute little to increasing the hopping time even if they are localized.

V. DISCUSSION AND SUMMARY

We have applied our theory [15] of coupled activated dynamics in biphasic mixtures to study how the effective free-energy surface, barriers, saddle-point trajectories, and mean first passage times depend on mixture composition, (high) total volume fraction, and strength of sticky particle attraction. Usually, but not always, the barrier for activated motion increases with the ratio of sticky to repulsive particle displacement (direction on the two-dimensional landscape) $\delta r_s/\delta r_g$. However, at intermediate values of $\delta r_s/\delta r_g$, the barrier often attains a broad plateau value and can even undergo a maximum at high sticky particle composition if the strength of attraction is modest.

In general there are three types of saddle-point trajectories or relaxation pathways: a pure sticky or pure repulsive particle displacement keeping the other species localized, and a cooperative motion involving a specific mix of repulsive and attractive particle displacements. For a purely repulsive particle trajectory, the barrier that must be surmounted grows monotonically with attractive particle composition but decreases monotonically with the strength of sticky particle attraction. The latter trend reflects the enhanced clustering of attractive particles as they become more sticky, which opens up extra free volume for repulsive particle motion. On the other hand, pure attractive particle trajectories encounter a barrier that monotonically increases with attraction strength since the physical bonds formed become stronger. The mean first passage times generally reflect the trends in barrier height, especially as the attraction strengths increase. However, there are dramatic exceptions associated with cooperative repulsive and attractive particle trajectories, which may have relatively large barriers but can still be competitive relaxation channels due to the greatly enhanced number of such trajectories near the saddle point.

Our focus has been on high total volume fraction biphasic mixtures. How our conclusions change if the total volume fraction is relatively low has not been studied. However, at significantly lower ϕ_T, strong coupling of spinodal demixing, kinetic arrest, and activated hopping dynamics may occur, and a "glass" in the traditional sense of excluded volume force dominated caging may no longer be realized.

To test our theoretical results computer simulations of model biphasic mixtures are necessary. Experimental studies of biphasic mixtures will also be informative. However, the further development and application of our theory via stochastic simulation of the two coupled nonlinear Langevin equations [12] is required in order to be able to compute time dependent properties that can be probed experimentally via confocal microscopy and/or dynamic scattering. Quantities and questions of interest include the mean square displacements, non-Gaussian parameters, the van Hove function, and length-scale-dependent decoupling of diffusion and relaxation. The mixture model has been generalized to address diffusion in the tracer limit [33]. Finally, the theory is applicable to mixtures composed of spheres of different diameters, whether sticky or purely repulsive, a problem recently studied by simulation [34] that also appears to be related to particle dynamics in a porous medium [32].

ACKNOWLEDGMENTS

This work was supported by the Nanoscale Science and Engineering Initiative of the National Science Foundation under NSF Grant No. DMR-0642573.

APPENDIX: CHARACTERISTIC LENGTHS, DISPLACEMENT RATIOS, AND ENERGY SCALES

The numerical values of all important features of the effective free energy surface, the elastic shear modulus, and mean first passage time of the systems studied in detail in Secs. II and IV are summarized in Tables I and II.

TABLE I. Numerical results for the displacement ratio of saddle point trajectories, localization lengths, barrier locations, elastic shear modulus (units of k_BT/D^3), and barrier height for several mixtures compositions and sticky particle attraction strengths for a total volume fraction of 0.45.

ϕ_s	$\delta r_s/\delta r_g$	ε_{ss}	$r_{L,g}$	$r_{B,g}$	$r_{L,s}$	$r_{B,s}$	G'	F_B
0.0	0	3.00	0.242	0.242			17.4	0.18
0.1	∞	3.00	0.116	0.116	0.094	1.263	18.7	6.47
0.1	0.3640	3.00	0.116	0.224	0.094	0.133	18.7	0.13
0.1	0	3.00	0.116	0.271	0.094	0.094	18.7	0.29
0.2	∞	3.00	0.113	0.113	0.003	0.825	4958	7.06
0.2	0.8693	3.00	0.113	0.236	0.003	0.110	4958	2.94
0.2	0	3.00	0.113	0.310	0.003	0.003	4958	0.55
0.3	∞	3.00			0.002	0.573		8.66
0.3	0	3.00	0.116	0.343				0.71
0.4	∞	3.00			0.002	0.466		9.70
0.4	0	3.00	0.117	0.378				0.88
0.5	∞	3.00	0.121	0.121	0.002	0.398	40422	10.04
0.5	1.3764	3.00	0.121	0.275	0.002	0.214	40422	9.19
0.5	0	3.00	0.121	0.423	0.002	0.002	40422	1.06
0.6	∞	3.00	0.127	0.127	0.002	0.355	51508	9.93
0.6	2.3559	3.00	0.127	0.229	0.002	0.242	51508	9.45
0.6	0	3.00	0.127	0.489	0.002	0.002	51508	1.30
0.7	∞	3.00	0.133	0.133	0.002	0.304	60473	9.51
0.7	3.4874	3.00	0.133	0.197	0.002	0.224	60473	9.25
0.7	0	3.00	0.133	0.591	0.002	0.002	60473	1.69
0.8	∞	3.00	0.141	0.141	0.002	0.238	67204	8.92
0.8	7.1154	3.00	0.141	0.167	0.002	0.191		8.80
0.8	0	3.00	0.141	0.804	0.002	0.002		2.40
0.9	∞	3.00	0.151	0.151	0.002	0.160	71901	8.30
0.9	6.3138	3.00	0.151	0.172	0.002	0.136		8.27
0.9	0	3.00	0.151	1.225	0.002	0.002		4.12
1.0	∞	3.00			0.002	0.111	74618	7.73
0.5	∞	2.75	0.116	0.116	0.003	0.409	13800	5.18
0.5	1.7321	2.75	0.116	0.248	0.003	0.232		4.29
0.5	0	2.75	0.116	0.432	0.003	0.003		1.22
0.8	∞	2.75	0.131	0.131	0.003	0.245	27506	4.77
0.8	5.6713	2.75	0.131	0.160	0.003	0.167		4.64
0.8	0	2.75	0.131	0.830	0.003	0.003		2.86
1.0	∞	2.75			0.003	0.090	32860	4.27
0.8	∞	3.50	0.165	0.165	0.001	0.240	190913	21.74
0.8	5.6713	3.50	0.165	0.202	0.001	0.210		21.61
0.8	0	3.50	0.165	0.738	0.001	0.738		1.54

TABLE II. Factors that enter the multidimensional Kramers theory expression for the mean first passage time of cooperative and pure species displacement trajectories for biphasic mixtures of total volume fraction 0.45. Results are shown for the prefactor in Eq. (14), barrier height, sticky to repulsive particle ratio of the short-time friction constant (G_s/G_g), ratio of contact values (g_{ss}/g_{gg}), and the mean first passage time.

ϕ_s	$\delta r_s/\delta r_g$	ε_{ss}	Prefactor	F_B	G_s/G_g	g_{ss}/g_{gg}	τ/τ_0
0.0	0	3.00	0.024	0.18	1.00	2.17	0.18
0.1	∞	3.00	0.367	6.47	2.68	18.24	1484.41
0.1	0.3640	3.00	0.010	0.13			0.07
0.1	0	3.00	0.024	0.29			0.20
0.2	∞	3.00	0.016	7.06	4.12	16.56	117.32
0.2	0.8693	3.00	0.0005	2.94			0.06
0.2	0	3.00	0.046	0.55			0.51
0.3	∞	3.00	0.007	8.66	5.38	15.07	269.42
0.3	0	3.00	0.047	0.71			0.60
0.4	∞	3.00	0.006	9.70	6.52	13.77	630.39
0.4	0	3.00	0.050	0.88			0.76
0.5	∞	3.00	0.006	10.04	7.60	12.62	810.73
0.5	1.3764	3.00	0.00002	9.19			0.99
0.5	0	3.00	0.054	1.06			0.98
0.6	∞	3.00	0.006	9.93	8.63	11.62	777.18
0.6	2.3559	3.00	0.0002	9.45			13.39
0.6	0	3.00	0.061	1.04			1.41
0.7	∞	3.00	0.007	9.51	9.67	10.75	569.32
0.7	3.4874	3.00	0.003	9.25			173.81
0.7	0	3.00	0.075	1.69			2.54
0.8	∞	3.00	0.008	8.92	10.72	9.98	375.18
0.8	7.1154	3.00	0.006	8.80			271.64
0.8	0	3.00	0.110	2.40			7.64
0.9	∞	3.00	0.009	8.30	11.83	9.30	219.21
0.9	6.3138	3.00	0.006	8.27			135.20
0.9	0	3.00	0.139	4.12			53.91
1.0	∞	3.00	0.005	7.73	13.01	8.69	73.64
0.5	∞	2.75	0.009	5.18	6.25	10.41	10.17
0.5	1.7321	2.75	0.0002	4.29			0.10
0.5	0	2.75	0.052	1.22			1.12
0.8	∞	2.75	0.011	4.77	8.82	8.46	8.60
0.8	5.6713	2.75	0.013	4.64			8.53
0.8	0	2.75	0.107	2.86			11.69
1.0	∞	2.75	0.006	4.27	10.69	7.47	2.74
0.8	∞	3.50	0.004	21.74	15.73	13.66	73514770
0.8	5.6713	3.50	0.003	21.61			38949470
0.8	0	3.50	0.116	1.54			3.42

[1] W. B. Russel, D. A. Saville, and W. R. Schowalter, *Colloidal Dispersions* (Cambridge University Press, Cambridge, 1991).
[2] R. G. Larson, *The Structure and Rheology of Complex Fluids* (Oxford University Press, New York, 1999).
[3] W. C. K. Poon, J. Phys.: Condens. Matter **14**, R859 (2002).
[4] K. A. Dawson, Curr. Opin. Colloid Interface Sci. **7**, 218 (2002); F. Sciortino, Nature Mater. **1**, 145 (2002).
[5] W. Götze and L. Sjögren, Rep. Prog. Phys. **55**, 241 (1992); W. Götze, J. Phys.: Condens. Matter **11**, A1 (1999).
[6] L. Fabbian, W. Götze, F. Sciortino, P. Tartaglia, and F. Thiery, Phys. Rev. E **59**, R1347 (1999).
[7] E. Zaccarelli, J. Phys.: Condens. Matter **19**, 323101 (2007); J. Bergenholtz and M. Fuchs, Phys. Rev. E **59**, 5706 (1999); J. Bergenholtz, W. Poon, and M. Fuchs, Langmuir **19**, 4493 (2003); K. Dawson, G. Foffi, M. Fuchs, W. Götze, F. Sciortino, M. Sperl, P. Tartaglia, T. Voigtmann, and E. Zaccarelli, Phys. Rev. E **63**, 011401 (2000); E. Zaccarelli, G. Foffi, K. A. Dawson, F. Sciortino, and P. Tartaglia, *ibid.* **63**, 031501 (2001).
[8] T. R. Kirkpatrick and P. G. Wolynes, Phys. Rev. A **35**, 3072 (1987).
[9] K. S. Schweizer and E. J. Saltzman, J. Chem. Phys. **119**, 1181 (2003).
[10] Y.-L. Chen and K. S. Schweizer, J. Chem. Phys. **120**, 7212 (2004).
[11] K. S. Schweizer, J. Chem. Phys. **123**, 244501 (2005).
[12] E. J. Saltzman and K. S. Schweizer, Phys. Rev. E **74**, 061501 (2006); J. Chem. Phys. **125**, 044509 (2006).
[13] K. S. Schweizer, Curr. Opin. Colloid Interface Sci. **12**, 297 (2007).
[14] Y.-L. Chen, V. Kobelev, and K. S. Schweizer, Phys. Rev. E **71**, 041405 (2005).
[15] D. C. Viehman and K. S. Schweizer, J. Chem. Phys. **128**, 084509 (2008).
[16] J. Bosse and J. S. Thakur, Phys. Rev. Lett. **59**, 998 (1987); J. S. Thakur and J. Bosse, Phys. Rev. A **43**, 4378 (1991); **43**, 4388 (1991); J. Bosse and Y. Kaneko, Phys. Rev. Lett. **74**, 4023 (1995).
[17] W. Götze and Th. Voigtmann, Phys. Rev. E **67**, 021502 (2003).
[18] G. Foffi, W. Götze, F. Sciortino, P. Tartaglia, and Th. Voigtmann, Phys. Rev. Lett. **91**, 085701 (2003); Phys. Rev. E **69**, 011505 (2004).
[19] E. Zaccarelli, H. Lowen, P. P. F. Wessels, F. Sciortino, P. Tartaglia, and C. N. Likos, Phys. Rev. Lett. **92**, 225703 (2004).
[20] Th. Voigtmann, Phys. Rev. E **68**, 051401 (2003).
[21] E. Zaccarelli, C. Mayer, A. Asteriadi, C. N. Likos, F. Sciortino, J. Roovers, H. Iatrou, N. Hadjichristidis, P. Tartaglia, H. Lowen, and D. Vlassopoulos, Phys. Rev. Lett. **95**, 268301 (2005).
[22] C. Mayer, E. Stiakakis, E. Zaccarelli, C. N. Likos, F. Sciortino, P. Tartaglia, H. Lowen, and D. Vlassopoulos, Rheol. Acta **46**, 611 (2007).
[23] K. N. Plunkett, A. Mohraz, R. T. Haasch, J. A. Lewis, and J. S. Moore, J. Am. Chem. Soc. **127**, 14574 (2005); A. Mohraz, E. R. Weeks, and J. A. Lewis, Phys. Rev. E **77**, 060403(R) (2008); R. Rao, Ph.D. thesis, University of Illinois, Urbana-Champaign, 2008; Q. Li, M.S. thesis, University of Illinois, Urbana-Champaign, 2005.
[24] G. Nägele and J. Bergenholtz, J. Chem. Phys. **108**, 9893 (1998).
[25] J. P. Hansen and I. R. McDonald, *Theory of Simple Liquids* (Academic, London, 1986).
[26] J. M. Méndez-Alcaraz and R. Klein, Phys. Rev. E **61**, 4095 (2000).
[27] J. A. Cuesta and Y. Martinez-Raton, J. Phys.: Condens. Matter **11**, 10107 (1999).
[28] P. Hänggi, P. Talkner, and M. Borkovec, Rev. Mod. Phys. **62**, 251 (1990).
[29] E. G. D. Cohen, R. Verberg, and I. M. de Schepper, Physica A **251**, 251 (1998); R. Verberg, I. M. deSchepper, and E. G. D. Cohen, Phys. Rev. E **55**, 3143 (1997).
[30] J. S. Langer, Ann. Phys. (N.Y.) **54**, 258 (1969).
[31] A. M. Berezhkovskii and A. Szabo, J. Chem. Phys. **122**, 014503 (2005).
[32] V. Krakoviack, Phys. Rev. Lett. **94**, 065703 (2005).
[33] D. C. Viehman and K. S. Schweizer, J. Phys. Chem. B (to be published).
[34] A. J. Moreno and J. Colmenero, J. Chem. Phys. **125**, 164507 (2006).